A microstructural approach to model heat transfer in snow

T. U. Kaempfer, M. Schneebeli, and S. A. Sokratov

WSL, Swiss Federal Institute for Snow and Avalanche Research SLF, Davos, Switzerland

[1] The relation between heat flow through snow and microstructure is crucial for the comprehension and modeling of thermophysical, chemical, and mechanical properties of snow. This relationship was investigated using heat flux measurements combined with a microstructural numerical approach. A snow sample was subjected to a temperature gradient and the passing heat flux was measured. Simultaneously, the snow microstructure was imaged by X-ray micro-tomography. The heat flow through the observed ice matrix and its heat conductivity was computed by a finite element method. Comparison of measured and simulated heat conductivities suggests that heat conduction through the ice matrix is predominant. The representative elementary volume with respect to density and heat conductivity as well as the tortuosity factor of the ice matrix was determined. In contrast to the density, the tortuosity factor takes into account the relevant geometry of the ice matrix and has many advantages in heat transfer models. **Citation:** Kaempfer, T. U., M. Schneebeli, and S. A. Sokratov (2005), A microstructural approach to model heat transfer in snow, *Geophys. Res. Lett.*, *32*, L21503, doi:10.1029/2005GL023873.

1. Introduction

[2] Heat flow through snow induces metamorphism and thus modifies the snow microstructure, which in turn influences the properties of snow [*Arons and Colbeck*, 1995]. These include thermophysical properties, important for modeling the energy balance of snow-covered landscapes [*Sokratov and Barry*, 2002]; chemical properties used for the interpretation of ice cores [*Legrand and Mayewski*, 1997]; and mechanical properties necessary for avalanche forecasting [*Schweizer et al.*, 2003]. An understanding of the relationship between heat flow and snow microstructure is thus crucial for improving models in climatology, interpretations of geochemical and isotopic signals, and avalanche research.

[3] Current heat transport models [*Sturm et al.*, 1997] relate the effective heat conductivity of snow, κ_s, empirically to the snow density. However, measured κ_s differ up to five times between measurements made in snow that is similar both in density and in crystal type [*Sturm et al.*, 1997]. It is thus necessary to find more relevant parameters related to the snow microstructure that govern κ_s. So far, the microstructural complexity always required simplifications, as for example in the model of *Adams and Sato* [1993], which uses uniformly packed ice spheres. Only recently did tomographic reconstructions [*Schneebeli*, 2000; *Brzoska et al.*, 1999] lead to 3D representations of the real snow structure at the micro-scale. *Schneebeli* [2004] uses such reconstructions to compute elastic stress in the ice matrix of snow, but no relation to heat transport has been established so far.

[4] We used the snow microstructure imaged by computed X-ray micro-tomography (μ-CT) to study heat transport through snow. We subjected a snow sample to a constant temperature gradient, $|\nabla T_g|$, measured the passing heat flux, and determined the effective heat conductivity of the snow. Simultaneously, we imaged the snow microstructure by μ-CT, as described by *Schneebeli and Sokratov* [2004], discretized the ice matrix by finite elements, and solved the stationary heat transport equation corresponding to the experimental setup. We deduced the representative elementary volume (REV) of the snow with respect to density and heat flux in the ice matrix and related it to microstructural parameters obtained by image analysis. Moreover, we determined the tortuosity factor of the ice matrix, which takes into account the heat transport in the ice matrix.

2. Experimental Setup

[5] We sieved snow into a cylindrical sample holder developed for temperature gradient metamorphism experiments inside the micro-tomograph [*Schneebeli and Sokratov*, 2004], resulting in a snow sample of 2 cm height and 4.8 cm in diameter. The final density, determined by weighting the sample, was $\rho_s = 268$ kg m^{-3}, and the snow type was small, rounded grains (class 3a in the international classification). We kept the temperature inside the μ-CT measurement chamber constant at $T_{\text{env}} = 265.6 \pm 0.5$ K and applied a temperature gradient of $|\nabla T_g| = 40 \pm 5$ K m^{-1} to the snow. We installed two heat flux sensors with a precision of ± 0.1 W m^{-2} at the top and bottom of the sample. Directly after imposing the temperature gradient and as soon as the flux measurements were stabilized, we determined the heat flux through the snow and imaged the snow using μ-CT with a spatial resolution of 25 μm. We deduced two microstructural parameters using the distance transform image analysis technique: the mean thickness of the ice matrix, *Tb.Th*, which is determined by filling maximal spheres into the structure and taking their average size [*Hildebrand and Rüegsegger*, 1997]; and the number of traversals of ice per unit length on a linear path through the structure, called trabecular number and noted *Tb.N*, which is given by the inverse of the mean distance between the medial axes of the ice structure [*Hildebrand et al.*, 1999].

3. Numerical Model

[6] We discretized the ice matrix of a sub-volume Ω of the snow by transforming each ice voxel to an eight-node brick finite element, leading to the computational domain
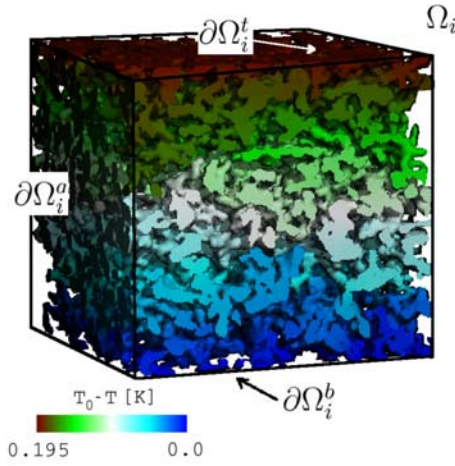
Figure 1. The computational domain Ω_i consisting of the ice matrix in the snow of class 3a, with the simulated temperature distribution. $\partial\Omega_i^b$ and $\partial\Omega_i^t$ are the bottom and top of the domain boundary $\partial\Omega_i$, respectively, while $\partial\Omega_i^a$ represents the remaining boundary. The shown domain has dimensions of $5 \times 5 \times 4.875$ mm, respectively $200 \times 200 \times 195$ voxels.

Ω_i. Let an orthonormal coordinate system $(O, \vec{e}_x, \vec{e}_y, \vec{e}_z)$, denote a point in Ω_i by $\vec{x} = (x, y, z)$, and suppose that $\vec{e}_z$ is oriented along the height of Ω_i and thus parallel to the applied heat flux. Denote the boundary of Ω_i by $\partial\Omega_i$ and set $\partial\Omega_i = \partial\Omega_i^t \cup \partial\Omega_i^b \cup \partial\Omega_i^a$, where the superscripts t and b stand for the top and bottom of Ω_i, while $\partial\Omega_i^a$ represents the remaining boundaries (Figure 1).

[7] We solved the stationary energy conservation equation within Ω_i:

$$\kappa_i \nabla^2 T(\vec{x}) = 0, \quad \vec{x} \in \Omega_i, \qquad (1)$$

where $T(\vec{x})$ is the temperature and $\kappa_i = 2.29$ W m^{-1} K^{-1} is the conductivity of pure, crystalline ice, supposed to be constant and taken as $\kappa_i = \kappa_i(T_{\text{env}})$ in the definition given by *Fukusako and Yamada* [1993]. The error on κ_i due to nonconstant temperatures is only $\pm 0.2\%$ and will be neglected. The boundary conditions were chosen to meet the experimental settings:

$$T = T_0, \quad \vec{x} \text{ on } \partial\Omega_i^b, \qquad (2)$$

$$T = T_1, \quad \vec{x} \text{ on } \partial\Omega_i^t, \qquad (3)$$

$$\frac{\partial T}{\partial \vec{n}} = 0, \quad \vec{x} \text{ on } \partial\Omega_i^a, \qquad (4)$$

where $\vec{n}$ denotes the outward normal on $\partial\Omega_i^a$, and T_0 and T_1 were chosen such that $|\nabla T_g^c| = \Delta T/h = \mu(|\nabla T_g|)$, with $\Delta T = T_0 - T_1$, h the height of Ω_i, and $\mu(|\nabla T_g|)$ the mean value of the experimental $|\nabla T_g|$. The homogeneous Neumann boundary condition (equation 4) corresponds to insulation at the outer walls of Ω_i as in the experiment and no heat exchange between ice and air, i.e., neglecting the pore space.

[8] The finite element code by *van Rietbergen et al.* [1995] is designed to compute elastic deformations in bones. By using the physical analogy between the Hook's and Fourier's laws we adapted the code to solve equations (1)–(4). The computation is based on a preconditioned conjugate gradient method and an element-by-element approach.

4. Results

4.1. Representative Elementary Volume and Structural Parameters

[9] The representative elementary volume (REV) of a material with respect to a macroscopic property is the minimal volume at which it is reasonable to define this property [*Brown et al.*, 2000].

[10] We determined the REV with respect to the density by using four cubic sub-volumes, within each of them we increased the computational volume size in $\vec{e}_x, \vec{e}(y), \vec{e}_z$ from the center on (Figure 2, left axis).

[11] To determine the REV with respect to the heat flux, we solved numerically the equations (1)–(4) for snow volumes with different sizes and at different positions. We kept the size in the direction of the heat flux, the $\vec{e}_z$-direction, constant equal to 195 voxels. In order to keep the computational time reasonable, we performed the following simulations: For dimensions in $\vec{e}_x, \vec{e}_y$ of 50×50, 124×124, and 200×200 voxels, we chose 10, 7, and 4 different regions, respectively, while we performed only one simulation (at one position) for domain sizes of 74, 150, 174, 224, and 250 voxels in $\vec{e}_x, \vec{e}_y$. The corresponding heat fluxes through the ice matrix are presented in Figure 2, right axis.

[12] Concerning the structural parameters, we determined the mean ice thickness $Tb.Th = 0.1$ mm and the trabecular number $Tb.N = 3.1$ mm^{-1} for the total volume of the observed snow.

4.2. Measured and Simulated Heat Transport

[13] The measured heat flux, $\vec{q}_s$, which was taken as the mean value given by the bottom and top heat flux sensors, was $|\vec{q}_s| = 7.2 \pm 0.1$ W m^{-2}. With the imposed temperature
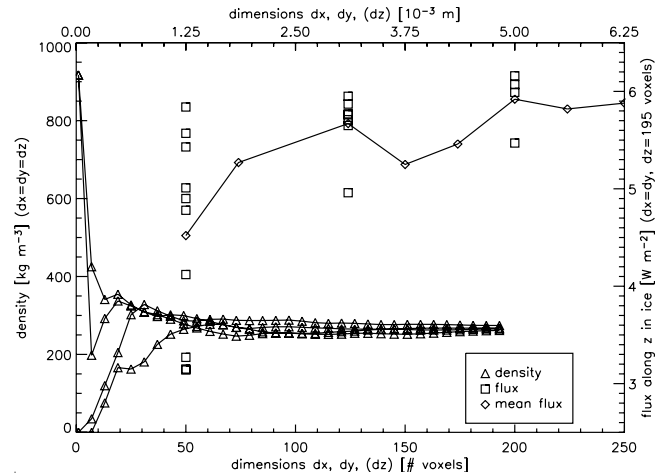

Figure 2. Density of the snow (left) and the computed heat flux through the ice matrix (right) for different snow sub-volumes and in function of the volume size.
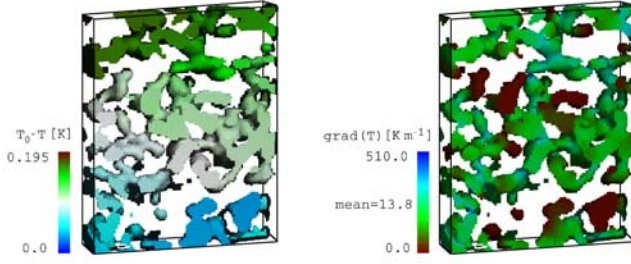
Figure 3. Computed temperature (left) and temperature gradient (right) in the ice matrix of a 2.25 × 0.3 × 2.7 mm (respectively 90 × 12 × 108 voxel) slice within the computational region.

gradient $|\nabla T_g| = 40 \pm 5$ K m^{-1} and by Fick's law, this corresponds to an experimental heat conductivity of $\kappa_s = 0.18 \pm 0.02$ W m^{-1} K^{-1}.

[14] Using the boundary conditions corresponding to the experiment with the mean temperature gradient $|\nabla T_g^c| = 40$ K m^{-1}, we computed the temperature distribution within the ice matrix, neglecting the pore space and any phase changes (Figure 1). The temperature and temperature gradient fields within a 2.25 × 0.3 × 2.7 mm sub-domain are shown enlarged in Figure 3.

[15] For each voxel, respectively finite element, the temperature gradient ∇T_c was determined from the computed temperature values at its nodes by linear approximation and an apparent heat flux along $\vec{e}_z$ through the snow, denoted $\vec{q}_i^s \cdot \vec{e}_z$, considering only conduction in the ice matrix, was computed by

$$\vec{q}_i^s \cdot \vec{e}_z = \frac{\int_{S_i} \vec{q}_i \cdot \vec{e}_z \, ds}{A_s}, \qquad (5)$$

where $\vec{q}_i = -\kappa_i \nabla T_c$ is the heat flux in the ice matrix, S_i is the ice matrix surface in any cross-section perpendicular to $\vec{e}_z$, and A_s is the total cross-section in $\vec{e}_x$, $\vec{e}_y$ of the computational domain. An apparent heat conductivity was deduced by setting $\kappa_c = \dfrac{\vec{q}_i^s \cdot \vec{e}_z}{|\nabla T_g^c|}$. For a computational volume of 250 × 250 × 195 voxels, we determined $\kappa_c = 0.15 \pm 0.01$ W m^{-1} K^{-1} for the studied snow, where the error estimate is related to the REV and the discretization as discussed below.

4.3. Tortuosity Factor

[16] The square of the ratio between the effective diffusion path, L_e, through a porous medium and its length along the major diffusion axis, L, is known as the tortuosity factor, τ^2 [Epstein, 1989]. If the porous medium is modeled by a bundle of sinuous but parallel capillaries or pores, L_e is the average pore length. If there is no well defined geometric diffusion path, one can still express the effective conductivity of the porous medium, κ_e, by the conductivity of the matrix, κ, by following the argumentation of Epstein [1989] and get $\kappa_e = \dfrac{\epsilon}{\tau^2}\kappa$, where ϵ is the volumetric density. This leads to $\tau^2 = \dfrac{\kappa\epsilon}{\kappa_e}$.

[17] We computed the tortuosity factor for the porous space in cubic lattices of densely packed, identical spheres

using a computational domain of 5^3 lattices, where each lattice had a spatial resolution in each direction $\vec{e}_x$, $\vec{e}_y$, $\vec{e}_z$ of 21 and 41 voxels. We compared the results with the values published by *Tallarek et al.* [1999] in Table 1; Their values are based on the analytical solution for the effective diffusion coefficient by *Venema et al.* [1991]. In addition, we determined a tortuosity factor of 2.01 for the sphere-structure of the BCC configuration.

[18] For the ice matrix, with $\kappa_e = \kappa_c = 0.15 \pm 0.01$ W m^{-1} K^{-1}, $\kappa = \kappa_i = 2.29$ W m^{-1} K^{-1}, and $\epsilon = \rho_s/\rho_i = 268/917 = 0.29$, we deduced a tortuosity factor $\tau_i^2 = \kappa_i\epsilon/\kappa_c = 4.4 \pm 0.3$.

5. Discussion

5.1. Representative Elementary Volume

[19] The density related REV of the studied snow was 1.25^3 mm^3 (Figure 2). *Coléou et al.* [2001] obtained values of 2.5^3 mm^3 for a crust and volumes around 1.5^3 mm^3 for wet grains, depth hoar, or partially faceted particles. That our REV estimation is somewhat smaller might be explained by the smaller grain size of our snow.

[20] A reasonable approximation of the REV with respect to the heat flux in the ice matrix, and thus to the tortuosity factor τ_i^2, was 5^3 mm^3. While the heat fluxes scattered considerably for smaller volumes, we computed here a mean heat flux of 5.92 W m^{-2} with a standard deviation of 0.31 W m^{-2} and are thus within a precision of ±5%. Considering the trabecular number of $Tb.N = 3.1$ mm^{-1}, the REV related to τ_i^2 corresponds thus to a volume of about 15 structural elements in each dimension. It is approximately 4^3 times larger than the REV with respect to density. Up to some extent this may be explained by boundary effects as some arms of the ice matrix end up at a side boundary and are thus a dead-end for the heat flux; but mainly it is explained by the high variability of ∇T_c in the ice matrix (Figure 3, right), which leads to a much larger averaging volume than for the density, where the averaging field is just binary.

5.2. Heat Transport Through the Ice Matrix

[21] The numerical model of *van Rietbergen et al.* [1995] adapted to heat transport through the ice matrix gave a heat conductivity which is expected from the direct measurement of heat conductivity in the snow. Considering the equivalence of the differential equations which were solved and the detailed discussion of the model limitations related to resolution, REV, and jagged interfaces by *van Rietbergen et al.* [1995], it remained to show that the discretization of our snow microstructure meets the criteria already established for bone. With the determined mean ice thickness of $Tb.Th = 0.1$ mm and the resolution of 25 μm, we reach a discretization of approximately 4 voxels per ice structure thickness. *van Rietbergen et al.* [1995] showed

Table 1. Tortuosity Factors of Porous Space in Cubic Lattices of Identical Spheres at Dense Packing Computed by Our Model Compared With the Ones Published by *Tallarek et al.* [1999]

Cubic Lattice	21 vox./Lattice	41 vox./Lattice	Published
SC	1.45	1.41	1.38
BCC	1.55	1.52	1.47
FCC	1.71	1.65	1.62

that, with this resolution, convergence in space was reached for stress and strain computations within a tolerance <2%. We confirmed this result by a numerical convergence test with respect to the apparent heat conductivity of the ice matrix.

[22] Analyzing the computed temperature distribution within the ice matrix, we note that high temperature differences of up to 20% of the overall ΔT occurred on a very short distance between one ice grain and another across a pore (Figure 3, left). This is due to the very tortuous structure of the ice matrix and leads to high temperature and vapor concentration gradients in the pores, which strongly influence metamorphism. High temperature gradients occurred also in the ice matrix (Figure 3, right).

5.3. Heat Conductivity

[23] Heat transport through snow is governed by heat conduction in the ice matrix and the pore space as well as by the heat transport associated with the water vapor diffusion. Convective effects can be neglected for the dimension of the snow sample and temperature gradient considered in this study, as an estimation of the Rayleigh number leads to $Ra \cong 1500$ [Zhao et al., 2005]. Comparison of the measured heat conductivity $\kappa_s = 0.18 \pm 0.02$ W m^{-1} K^{-1} with the computed one $\kappa_c = 0.15 \pm 0.01$ W m^{-1} K^{-1} suggests that conduction through the ice matrix was predominant and in the order of 80% of the overall heat flow. This estimate might vary for other snow types and densities and has to be interpreted carefully, as some errors with respect to the idealized model were neglected. These include possible variations in the heat conductivity of ice, imperfect boundary conditions, or errors related to the image analysis procedures. The completion of the numerical model by water vapor diffusion will help to answer the question on the relative importance of the heat conduction mechanisms.

[24] Note that Sturm et al. [1997] measured for snow of the same class (3a) and with similar density to our experiment values of κ_s between 0.15 and 0.18 W m^{-1} K^{-1}, while the empirical model gives $\kappa_s = 0.10$ W m^{-1} K^{-1}, with a 95% confidence interval of approximately ± 0.1 W m^{-1} K^{-1}.

5.4. Tortuosity Factor

[25] By the simple solution of the heat equation on the ice structure observed by μ-CT, we deduced a microstructural parameter of snow which is per definition directly related to the heat flux: the tortuosity factor τ_i^2. By comparing computed tortuosity factors for cubic lattices with published values (Table 1), we conclude that for a resolution of 41 voxels per lattice, which corresponds roughly to having 4 voxels per structure-branch, we are within a precision of $\pm 1.9 - 3.4\%$, depending on the lattice structure. The fact that our computed values are systematically higher might be explained by discretization artefacts which result in contacts between spheres corresponding to disks instead of infinitesimal point contacts.

[26] The computed tortuosity factor of the ice-matrix $\tau_i^2 = 4.4 \pm 0.3$ was much larger compared to spherical beds in a BCC-configuration ($\tau^2 = 2.01$) and to an isotropic porous medium (2.0 [Epstein, 1989]). Classical geometrical models for snow microstructure assume either

a BCC or FCC configuration [Adams and Sato, 1993; Baunach et al., 2001] which cannot be justified based on our computations.

6. Conclusion

[27] The effective heat conductivity of the ice matrix in snow samples, even of very complex and layered texture, can be simulated and the tortuosity factor of the ice matrix can be deduced. The calculated tortuosity factor is very high, even for the texturally simple snow type investigated, compared to a material with a simple BCC-structure. Even higher tortuosity factors must be expected for texturally more complex snow types such as depth hoar. The high tortuosity causes, on very short distances across the pores, high temperature gradients and high vapor fluxes which strongly influence the metamorphic process. In a simple extension, using the analogy between Fourier's law and Darcy's law, the air permeability of snow can be calculated. The effective heat conductivity and the air permeability can be determined directly, if a measured three-dimensional snow structure is available.

References

Adams, E. E., and A. Sato (1993), Model for effective thermal conductivity of a dry snow cover composed of uniform ice spheres, Ann. Glaciol., 18, 300–304.

Arons, E. M., and S. C. Colbeck (1995), Geometry of heat and mass transfer in dry snow: A review of theory and experiment, Rev. Geophys., 33(4), 463–493.

Baunach, T., C. Fierz, P. K. Satyawali, and M. Schneebeli (2001), A model for kinetic grain growth, Ann. Glaciol., 32, 1–6.

Brown, G., H. Hsieh, and D. A. Lucero (2000), Evaluation of laboratory dolomite core sample size using representative elementary volume concepts, Water Resour. Res., 36(5), 1199–1207.

Brzoska, J.-B., C. Coléou, B. Lesaffre, S. Borel, O. Brissaud, W. Ludwig, E. Boller, and J. Baruchel (1999), 3d visualization of snow samples by microtomography at low temperature, Eur. Synchrotron Radiat. Facil. Newsl., 32, 22–23.

Coléou, C., B. Lesaffre, J.-B. Brzoska, W. Ludwig, and E. Boller (2001), Three-dimensional snow images by X-ray microtomography, Ann. Glaciol., 32, 75–81.

Epstein, N. (1989), On tortuosity and the tortuosity factor in flow and diffusion through porous media, Chem. Eng. Sci., 44(3), 777–779.

Fukusako, S., and M. Yamada (1993), Recent advances in research on water-freezing and ice-melting problems, Exp. Therm Fluid Sci., 6(1), 90–105.

Hildebrand, T., and P. Rüegsegger (1997), A new method for the model-independent assessment of thickness in three-dimensional images, J. Microsc., 185(1), 67–75.

Hildebrand, T., A. Laib, R. Müller, J. Dequeker, and P. Rüegsegger (1999), Direct three-dimensional morphometric analysis of human cancellous bone: Microstructural data from spine, femur, iliac crest, and calcaneus, J. Bone Miner. Res., 14(7), 1167–1174.

Legrand, M., and P. Mayewski (1997), Glaciochemistry of polar ice cores: A review, Rev. Geophys., 35(3), 219–243.

Schneebeli, M. (2000), Three-dimensional snow: How snow really looks like, paper presented at International Snow Science Workshop, Mont. State Univ., Big Sky, Mont.

Schneebeli, M. (2004), Numerical simulation of elastic stress in the microstructure of snow, Ann. Glaciol., 38, 339–342.

Schneebeli, M., and S. A. Sokratov (2004), Tomography of temperature gradient metamorphism of snow and associated changes in heat conductivity, Hydrol. Processes, 18(18), 3655–3665, doi:10.1002/hyp.5800.

Schweizer, J., J. B. Jamieson, and M. Schneebeli (2003), Snow avalanche formation, Rev. Geophys., 41(4), 1016, doi:10.1029/2002RG000123.

Sokratov, S. A., and R. G. Barry (2002), Intraseasonal variation in the thermoinsulation effect of snow cover on soil temperatures and energy balance, *J. Geophys. Res.*, *107*(D10), 4093, doi:10.1029/2001JD000489.

Sturm, M., J. Holmgren, M. König, and K. Morris (1997), The thermal conductivity of seasonal snow, *J. Glaciol.*, *43*(143), 26–41.

Tallarek, U., F. J. Vergeldt, and H. Van As (1999), Stagnant mobile phase mass transfer in chromatographic media: Intraparticle diffusion and exchange kinetics, *J. Phys. Chem. B*, *103*, 7654–7664.

van Rietbergen, B., H. Weinans, R. Huiskes, and A. Odgaard (1995), A new method to determine trabecular bone elastic properties and loading using micromechanical finite-element models, *J. Biomech.*, *28*(1), 69–81.

Venema, P., R. P. W. J. Struis, J. C. Leyte, and D. Bedeaux (1991), The effective self-diffusion coefficient of solvent molecules in colloidal crystals, *J. Colloid Interface Sci.*, *141*(2), 360–373.

Zhao, C. Y., T. J. Lu, and H. P. Hodson (2005), Natural convection in metal foams with open cells, *Int. J. Heat Mass Transfer*, *48*, 2452–2463.

———————————

T. U. Kaempfer, M. Schneebeli, and S. A. Sokratov, WSL, Swiss Federal Institute for Snow and Avalanche Research SLF, Flüelastrasse 11, CH-7260 Davos Dorf, Switzerland. (kaempfer@slf.ch; schneebeli@slf.ch; sokratov@geol.msu.ru)